Real-Time Mobility Tracking Algorithms for Cellular Networks Based on Kalman Filtering

Zainab R. Zaidi, *Student Member*, *IEEE*, and Brian L. Mark, *Member*, *IEEE*

Abstract—We propose two algorithms for real-time tracking of the location and dynamic motion of a mobile station in a cellular network using the pilot signal strengths from neighboring base stations. The underlying mobility model is based on a dynamic linear system driven by a discrete command process that determines the mobile station's acceleration. The command process is modeled as a semi-Markov process over a finite set of acceleration levels. The first algorithm consists of an averaging filter for processing pilot signal strength measurements and two Kalman filters, one to estimate the discrete command process and the other to estimate the mobility state. The second algorithm employs a single Kalman filter without prefiltering and is able to track a mobile station even when a limited set of pilot signal measurements is available. Both of the proposed tracking algorithms can be used to predict future mobility behavior, which can be useful in resource allocation applications. Our numerical results show that the proposed tracking algorithms perform accurately over a wide range of mobility parameter values.

Index Terms—Cellular networks, mobility model, geolocation, pilot signal strengths, Kalman filter.

1 Introduction

As wireless services become more pervasive and location-aware, the need to locate and track mobile stations accurately and efficiently becomes increasingly important. A key technical challenge for modern wireless networks is to provide seamless access and quality-of-service (QoS) guarantees for mobile users. QoS provisioning can only be achieved by means of efficient mobility management to handle the frequent handoffs and rerouting of traffic that are experienced by a typical mobile station. We distinguish between mobility tracking, in which the position, velocity, and acceleration of the mobile user are estimated, versus conventional geolocation techniques, which only estimate the position coordinates. Knowledge of velocity and acceleration information can be used to predict the future locations of the mobile stations, which in turn can be used to optimize resource allocation in the network.

One application of great practical interest is fast handoff in cellular networks. If the occurrence of a handoff from one cell to another can be predicted ahead of time, the handoff procedure can be initiated in advance [1], [2]. These predictions can provide a "handoff pretrigger" incorporated in IP mobility protocols discussed in [3], [4], to provide transparent network layer mobility management. Another application area of interest is location-aware services, for example, E911 and Web caching (cf. [5]). In such applications, better quality-of-service can be achieved if the location of the mobile can be predicted in advance, even on a short time-scale.

Many geolocation technologies have been developed that can pinpoint the position of a mobile user on the surface of the earth. The most popular technology in current use, the Global Positioning System (GPS), provides the user with position estimates accurate to within a radius of 10 meters or better by means of at least four satellites from a system of 24 satellites, spaced equally in six orbital planes [6], [7]. To operate properly, however, GPS receivers require a clear view of the sky, in the line-of-sight of the satellites, which precludes their use in indoor or RF-shadowed environments. Moreover, the cost and size of GPS receivers may be prohibitive for small devices (e.g., sensors) with very limited battery lives that may be used in pervasive computing environments. Assisted GPS (AGPS) [8], [9] can work in indoor environments as well as outdoors, but this technology requires additional signaling equipment, i.e., AGPS receivers.

Geo-location techniques based on time of arrival (TOA), time difference of arrival (TDOA) [10], angle of arrival (AOA) [11], [12], timing advance, and location fingerprinting [13] offer inexpensive network-based alternatives to GPS, but are far less accurate. These techniques use the radio signals transmitted by the users instead of additional satellite signals. However, some of these techniques have additional infrastructure requirements; for example, AOA requires an adaptive antenna array to measure the angle of arrival and the location fingerprinting scheme requires a large amount of memory to maintain a location database.

While geolocation techniques focus on pinpointing the location of the user at a given instant of time, mobility tracking requires an underlying model to characterize the user's mobility. Construction of mobility patterns for analysis and simulation has attracted considerable attention in recent years (cf. [14], [15], [16], [17]). Such models can be used to drive simulation models of the wireless network. Several works have modeled mobile behavior as a random walk or Brownian motion [18]. In [19], a stochastic model of mobility based on a pair of coupled differential equations called the Markovian highway Poisson arrival location model (PALM) is proposed. A semi-Markov model proposed in [5] incorporates user mobility and requirements. The aforementioned mobility models, while useful for driving simulations of

• *The authors are with the Department of Electrical and Computer Engineering, MS 1G5, George Mason University, 4400 University Drive, Fairfax, VA 22030. E-mail: {zzaidi, bmark}@gmu.edu.*

Manuscript received 25 Feb. 2003; revised 15 Dec. 2003; accepted 20 Feb. 2004; published online 27 Jan. 2005.
For information on obtaining reprints of this article, please send e-mail to: tmc@computer.org, and reference IEEECS Log Number TMC-0023-0203.

mobile networks, have limitations in the range of mobility that can be captured. To our knowledge, none of these models is suitable for tracking the velocity and acceleration of a mobile station in real-time.

Liu et al. [1] proposed a mobility model for wireless ATM networks based on a dynamic linear system model in which the mobility state consists of the position, velocity, and acceleration of the mobile. Originally introduced by Singer [20] (cf. [21]) for tracking targets in tactical weapons systems, the dynamic system model can capture a wide range of realistic user mobility patterns. Based on this model, Liu et al. [1] developed an algorithm (which we refer to as the LBC algorithm) for estimating the mobility state using a modified Kalman filter with observations taken from three independent pilot signal strength measurements, also called RSSI (Received Signal Strength Indication) measurements, from three different base stations. In our numerical experiments, we have found that the LBC algorithm can perform poorly, particularly when the mobile trajectory includes rapid changes in acceleration. As discussed later in this paper, the poor performance of the LBC algorithm is due to some inaccurate assumptions in the estimation process.

The inaccuracy of the LBC estimator has also been pointed out by Yang and Wang [2], who proposed an alternative estimation scheme based on sequential Monte Carlo (SMC) filtering. The SMC scheme can achieve better performance than the LBC scheme, but is computationally intensive and, hence, might not be suitable for real-time location tracking. The SMC scheme relies on updating and storing a large number of sample weights. Moreover, the SMC scheme can suffer from numerical instability, which necessitates the use of a resampling procedure [2]. However, we have observed that resampling does not solve the problem completely and the estimation sometimes has to be terminated prematurely. A comparison of the performance of the SMC algorithm and the mobility estimators proposed in this paper is provided in Section 5.

In this paper, we propose two new mobility tracking algorithms based on RSSI measurements and Kalman filtering.[1] The first algorithm, which we call MT-1, differs from the LBC algorithm in that the RSSI measurements are preprocessed with an averaging filter to obtain coarse position estimates, which are then provided as inputs to a modified Kalman filter. In contrast to the LBC algorithm, the modified Kalman filter is used only to generate estimates of the discrete command process. A key component of the MT-1 algorithm is a second Kalman filter, which produces mobility state estimates from the raw RSSI measurements and the discrete command estimates. Our numerical results show that the MT-1 algorithm performs far more accurately than the LBC algorithm. The rationale behind the performance improvement is discussed later in the paper.

Our tracking algorithms can also utilize alternative types of observation data such as time-of-arrival (TOA) information or coarse tracking information obtained from GPS. Several schemes have been developed for estimation of TOA parameters from received signals such as code tracking and acquisition in spread spectrum systems using delay lock loop (DLL) or tau-dither loop as described in [23]. Moreover, the GPS receivers can be used to provide coarse location information, whenever available, to estimate the mobility state of the mobile station.

In the present paper, we also show how the mobility model can be used to predict the mobile's future movements. Mobility prediction can be used in resource management algorithms that preallocate resources in anticipation of the future position of the mobile user. In realistic mobile networking scenarios, there may be limitations on the amount of observation data available. We consider two such limitations: 1) RSSI measurement samples from a given base station may not be available at every time slot and 2) fewer than three independent RSSI measurements may be available. In the first case, there may be an insufficient number of observation samples to perform the averaging properly, as required in the MT-1 algorithm.

To avoid this problem, we propose a simplified mobility tracking algorithm called MT-2, which consists of only a single (extended) Kalman filter, without a prefilter. For the second limitation on observation data, mobility tracking may still be possible due to the inherent prior knowledge retained in the estimation process. This issue is discussed later in the paper using the concept of observability from systems theory. Our numerical results show that the MT-2 estimator is able to track mobility adequately with only two RSSI observations, even when the availability of measurement samples precludes the use of the MT-1 estimator. When the above limitations on observation data are not present, MT-1 performs better than MT-2. Both MT-1 and MT-2 outperform the LBC algorithm under a wide range of mobility scenarios.

Section 2 discusses the dynamic linear system mobility model on which our mobility tracking algorithms are based. Section 3 presents our proposed MT-1 and MT-2 mobility tracking algorithms and discusses how mobility behavior can be predicted under the dynamic mobility model. We point out why the LBC algorithm performs poorly and justify our proposed schemes for mobility tracking. Section 4 discusses issues related to mobility tracking under limited observation data. Section 5 presents numerical results demonstrating the accuracy and robustness of our proposed mobility tracking algorithms. Finally, Section 6 concludes the paper.

2 Dynamic Mobility State Model

In this section, we discuss a dynamic mobility state model that was originally developed for tracking maneuvering targets in tactical weapons systems [20], [21]. The mobility state model can capture a wide range of mobility scenarios, including sudden stops and changes in acceleration. More recently, Liu et al. [1] applied the model to characterize the mobility of a mobile station in a wireless ATM network. Our discussion is based on [1], but we correct several errors which appeared in that paper.

The mobile station's state at time t is defined by a (column) vector[2]

$$\boldsymbol{s}(t) = [x(t), \dot{\boldsymbol{x}}(t), \ddot{\boldsymbol{x}}(t), y(t), \dot{\boldsymbol{y}}(t), \ddot{\boldsymbol{y}}(t)]', \tag{1}$$

where $x(t)$ and $y(t)$ specify the position, $\dot{\boldsymbol{x}}(t)$ and $\dot{\boldsymbol{y}}(t)$ specify the velocity, and $\ddot{\boldsymbol{x}}(t)$ and $\ddot{\boldsymbol{y}}(t)$ specify the acceleration in the x

1. A preliminary version of this work appeared in [22].

2. The notation $'$ indicates the matrix transpose operator.

and y directions in a two-dimensional grid. The state vector can be written more compactly as

$$\boldsymbol{s}(t) = \begin{bmatrix} \boldsymbol{x}(t) \\ \boldsymbol{y}(t) \end{bmatrix}, \tag{2}$$

where $\boldsymbol{x}(t) = [x(t), \dot{x}(t), \ddot{x}(t)]'$ and $\boldsymbol{y}(t) = [y(t), \dot{y}(t), \ddot{y}(t)]'$.

The acceleration vector, $\boldsymbol{a}(t) = [\ddot{x}(t), \ddot{y}(t)]'$, is modeled as follows:

$$\boldsymbol{a}(t) = \boldsymbol{u}(t) + \boldsymbol{r}(t), \tag{3}$$

where $\boldsymbol{u}(t) = [u_x(t), u_y(t)]'$ is a discrete command process and $\boldsymbol{r}(t) = [r_x(t), r_y(t)]'$ is a zero-mean Gaussian process chosen to cover the gaps between adjacent levels of the process $\boldsymbol{u}(t)$. The command processes $u_x(t)$ and $u_y(t)$ are modeled as semi-Markov processes that take values from a finite set of acceleration levels $\mathcal{L} = \{l_1, \cdots, l_m\}$. Thus, the process $\boldsymbol{u}(t)$ takes values in the set $\mathcal{M} = \mathcal{L} \times \mathcal{L}$. The autocorrelation function of $\boldsymbol{r}(t)$ is given by

$$R_r(\tau) = E[\boldsymbol{r}(t)\boldsymbol{r}'(t+\tau)] = \sigma_1^2 e^{-\alpha|\tau|} I_2, \tag{4}$$

where σ_1^2 is the common variance of $r_x(t)$ and $r_y(t)$, α is the reciprocal of the acceleration time constant, and I_k denotes the $k \times k$ identity matrix for any positive integer k.

The process $\boldsymbol{r}(t)$ can be generated by passing a zero-mean, white Gaussian random process, $\boldsymbol{w}(t) = [w_x(t), w_y(t)]'$, through a single pole filter as follows:

$$\dot{\boldsymbol{r}}(t) = -\alpha \boldsymbol{r}(t) + \boldsymbol{w}(t). \tag{5}$$

The autocorrelation function of $\boldsymbol{w}(t)$ is given by

$$R_w(\tau) = 2\alpha\sigma_1^2 \delta(\tau) I_2, \tag{6}$$

where $\delta(\tau)$ is the Dirac delta function. Using (5), the linear system describing the state evolution in the x-direction can be written as:

$$\dot{\boldsymbol{x}}(t) = \tilde{A}_1 \boldsymbol{x}(t) + \tilde{B}_1 u_x(t) + \tilde{C}_1 w_x(t), \tag{7}$$

where

$$\tilde{A}_1 = \begin{bmatrix} 0 & 1 & 0 \\ 0 & 0 & 1 \\ 0 & 0 & -\alpha \end{bmatrix}, \tilde{B}_1 = \begin{bmatrix} 0 \\ 0 \\ \alpha \end{bmatrix}, \tilde{C}_1 = \begin{bmatrix} 0 \\ 0 \\ 1 \end{bmatrix}. \tag{8}$$

Similarly, the state equation for the y-direction is given by

$$\dot{\boldsymbol{y}}(t) = \tilde{A}_1 \boldsymbol{y}(t) + \tilde{B}_1 u_y(t) + \tilde{C}_1 w_y(t). \tag{9}$$

Combining (7) and (9) yields the overall state equation

$$\dot{\boldsymbol{s}}(t) = \tilde{A}\boldsymbol{s}(t) + \tilde{B}\boldsymbol{u}(t) + \tilde{C}\boldsymbol{w}(t), \tag{10}$$

where[3]

$$\tilde{A} = I_2 \otimes \tilde{A}_1, \tilde{B} = I_2 \otimes \tilde{B}_1, \tilde{C} = I_2 \otimes \tilde{C}_1, \tag{11}$$

and $\otimes$ denotes the Kronecker matrix product (cf. [24]).

By sampling the state once every T time units, the system can be characterized in terms of the discrete-time state vector $\boldsymbol{s}_n = \boldsymbol{s}(nT)$. The corresponding discrete-time state equation is given by

$$\boldsymbol{s}_{n+1} = A\boldsymbol{s}_n + B\boldsymbol{u}_n + \boldsymbol{w}_n, \tag{12}$$

where

$$A = e^{\tilde{A}T}, B = \int_t^{t+T} e^{\tilde{A}(t+T-\tau)} \tilde{B} d\tau \tag{13}$$

and

$$\boldsymbol{w}_n = \int_{nT}^{(n+1)T} e^{\tilde{A}(t+T-\tau)} \tilde{C}\boldsymbol{w}(\tau) d\tau. \tag{14}$$

The vector $\boldsymbol{w}_n$ is a 6×1 column vector.[4] The matrices A and B are given in Appendix A. The process $\boldsymbol{w}_n$ is a discrete-time zero mean, stationary Gaussian process with autocorrelation function $R_w(k) = \delta_k Q$, where $\delta_0 = 1$ and $\delta_k = 0$ when $k \neq 0$ [20]. The matrix Q, the covariance matrix of $\boldsymbol{w}_n$, is given in Appendix B.

In a cellular network, the distance between the mobile unit and a reachable base station can be inferred from the Received Signal Strength Indication (RSSI) or pilot signal of the base station. The RSSI, measured in dB, is typically modeled as the sum of three terms: path loss, shadow fading, and fast fading. Fast fading is assumed to be sufficiently attenuated using a low pass filter. Therefore, the RSSI received at the mobile unit from the base station in cell i with coordinates (a_i, b_i) at time n is given by (cf. [25], [26], [27], [28])

$$p_{n,i} = \kappa_i - 10\gamma \log(d_{n,i}) + \psi_{n,i}, \tag{15}$$

where κ_i is a constant determined by the transmitted power, wavelength, antenna height, and gain of cell i, γ is a slope index (typically, $\gamma = 2$ for highways and $\gamma = 4$ for microcells in a city), $\psi_{n,i}$ is a zero mean, stationary Gaussian process with standard deviation σ_ψ typically from 4-8 dB, and $d_{n,i}$ is the distance between the mobile unit and the base station, given by

$$d_{n,i} = \sqrt{(x_n - a_i)^2 + (y_n - b_i)^2}. \tag{16}$$

To locate the mobile station in the two-dimensional plane, three distance measurements to neighboring base stations are sufficient. Thus, the observation vector consists of the three largest RSSIs denoted $p_{n,1}$, $p_{n,2}$, $p_{n,3}$, given as follows:

$$\boldsymbol{o}_n = (p_{n,1}, p_{n,2}, p_{n,3})' = h(\boldsymbol{s}_n) + \boldsymbol{\psi}_n, \tag{17}$$

where $\boldsymbol{\psi}_n = (\psi_{n,1}, \psi_{n,2}, \psi_{n,3})'$ and

$$h(\boldsymbol{s}_n) = \boldsymbol{\kappa} - 10\gamma \log(\boldsymbol{d}_n), \tag{18}$$

where $\boldsymbol{\kappa} = (\kappa_1, \kappa_2, \kappa_3)'$ and $\boldsymbol{d}_n = (d_{n,1}, d_{n,2}, d_{n,3})'$. The covariance matrix of $\boldsymbol{\psi}_n$ is given by $R = \sigma_\psi^2 I_3$.

To estimate the mobility state vector $\boldsymbol{s}_n$, the observation equation, (17), is linearized as follows:[5]

$$\boldsymbol{o}_n = h(\boldsymbol{s}_n^*) + H_n \Delta\boldsymbol{s}_n + \boldsymbol{\psi}_n, \tag{19}$$

where $\boldsymbol{s}_n^*$ is the nominal or reference vector and $\Delta\boldsymbol{s}_n = \boldsymbol{s}_n - \boldsymbol{s}_n^*$ is the difference between the true and nominal state vectors. In an extended Kalman filter,[6] the nominal vector is

3. The expression for the matrix corresponding to $\tilde{B}$ on p. 934 of [1] is incorrect.

4. The corresponding vector W_n in (4) of [1] is incorrectly indicated as a 2×1 matrix.

5. The corresponding (8) in [1] is incorrect (cf. [7]).

6. In this context, the term "extended" refers to the linearized observation equation (cf. [7]).

obtained from the estimated state trajectory $\hat{\boldsymbol{s}}_n$, i.e., $\boldsymbol{s}_n^* = \hat{\boldsymbol{s}}_n$. The matrix H_n is given by

$$H_n = \frac{\partial h}{\partial \boldsymbol{s}}|_{\boldsymbol{s}=\hat{\boldsymbol{s}}_n}. \tag{20}$$

An explicit expression for H_n is given in Appendix C.

We assumed that the model parameters, i.e., κ_i, γ, and σ_ψ are known constants for our simulation studies. These parameters, however, may vary over a serving area. In practice, the base stations in many modern cellular networks (e.g., Sprint PCS) are capable of estimating the propagation model parameters γ and σ_ψ using the training field data consisting of pilot signals, mobile's location information, terrain information, etc. The parameter κ_i can be determined from the transmission characteristics of the base station i. As an example, the "deciBel Planner" software [29] developed by Northwood Technologies[7] provides this capability.

We also note that the mobility tracking algorithms described in this paper can use signal measurements other than RSSI. For example, some networks provide time-of-arrival (TOA) information [23]. If TOA information were used, (17) and (19) would change. An advantage of TOA is that we would not have to rely on the signal propagation model described in (15). On the other hand, TOA measurements require additional infrastructure involving delay lock loops.

3 Mobility Tracking Algorithms

In this section, we present two mobility tracking algorithms, MT-1 and MT-2, and discuss their accuracy and effectiveness in comparison with the LBC algorithm. We also describe how the algorithms can be used to predict the mobile's future trajectory.

3.1 MT-1 Algorithm

Fig. 1a illustrates the overall structure of our proposed MT-1 mobility estimator, consisting of a prefilter, a modified Kalman filter, and an extended Kalman filter.

3.1.1 Prefilter

The prefilter consists of an averaging filter and a coarse position estimator, as shown in Fig. 1b. The prefilter outputs a vector of position estimates denoted by $\hat{\boldsymbol{o}}_n = [\hat{x}_n, \hat{y}_n]'$, which are used as the observation data for the modified Kalman filter. The averaging filter reduces the shadowing noise considerably, without significantly modifying the path loss. The averaged RSSI measurements are then used to generate coarse estimates of the position coordinates.

The observation vector $\boldsymbol{o}_n$ as given in (17) consists of the path loss and the shadowing component. The averaging filter reduces the shadowing component in the observations. Different filters can be used for this purpose. Applying a rectangular window, the output $\tilde{\boldsymbol{o}}_n$ of the averaging filter is given as

$$\tilde{\boldsymbol{o}}_n = \frac{1}{N}\sum_{i=n-N+1}^{n} \boldsymbol{o}_i, \tag{21}$$

7. Now part of Marconi Wireless.

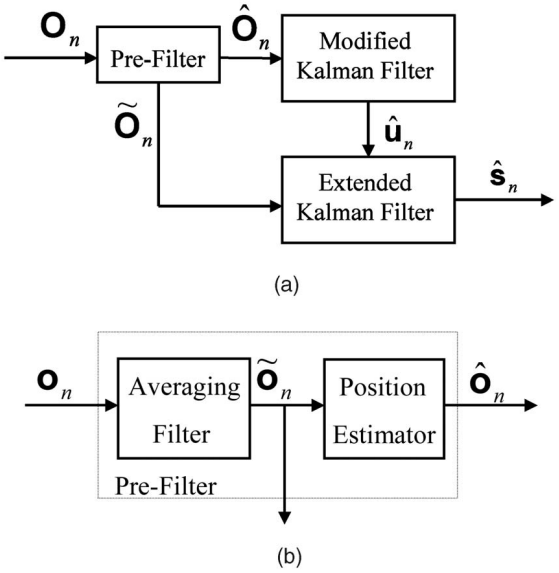

Fig. 1. Block diagram of MT-1 estimator. (a) Overall block diagram. (b) Prefiltering module.

where N is the length of the window. For small N, the residual shadowing component is quite large and yields erroneous position estimates; however, for large N, the path loss is modified and induces errors in the position estimates. Our solution to this problem is to use a bank of averaging filters in series, each with small length N, instead of a single filter of larger length. In the filter bank arrangement, each filter performs an averaging operation according to (21) and provides its output as input to the next filter in series.

This averaging scheme preserves path loss and reduces shadowing noise to a satisfactory level. Results using this averaging scheme are shown in Fig. 2. The parameter values are selected according to the *high mobility scenario* discussed in Section 5 with shadowing standard deviation set to 6 dB. The upper plot shows the averaged signal strength and actual path loss of the mobile.

The averaged observations $\tilde{\boldsymbol{o}}_n$ are used to generate coarse position coordinates $\hat{\boldsymbol{o}}_n = [\hat{x}_n, \hat{y}_n]'$, which are obtained as follows:

$$\begin{bmatrix} a_1 - a_2 & b_1 - b_2 \\ a_1 - a_3 & b_1 - b_3 \end{bmatrix} \begin{bmatrix} \hat{x}_n \\ \hat{y}_n \end{bmatrix} = 0.5 \begin{bmatrix} -e^{\frac{\kappa_1 - \tilde{\boldsymbol{o}}_n(1)}{5\gamma}} + e^{\frac{\kappa_2 - \tilde{\boldsymbol{o}}_n(2)}{5\gamma}} + a_1^2 - a_2^2 + b_1^2 - b_2^2 \\ -e^{\frac{\kappa_1 - \tilde{\boldsymbol{o}}_n(1)}{5\gamma}} + e^{\frac{\kappa_3 - \tilde{\boldsymbol{o}}_n(3)}{5\gamma}} + a_1^2 - a_3^2 + b_1^2 - b_3^2 \end{bmatrix},$$

where $(a_i, b_i), i = 1, 2, 3$ are the base station coordinates for cell i. Fig. 2b shows the estimates of position generated from the averaged RSSI and the actual position in 2-dimensional coordinates.

From the linear dynamic mobility model, it can be shown that the probability density function of the prefiltered observation vector $\hat{\boldsymbol{o}}_n$ conditioned on $\hat{\boldsymbol{O}}_{n-1}$, i.e., $f(\hat{\boldsymbol{o}}_n|\hat{\boldsymbol{O}}_{n-1})$, is approximately Gaussian. This property is crucial in the application of the modified Kalman filter to be discussed next.

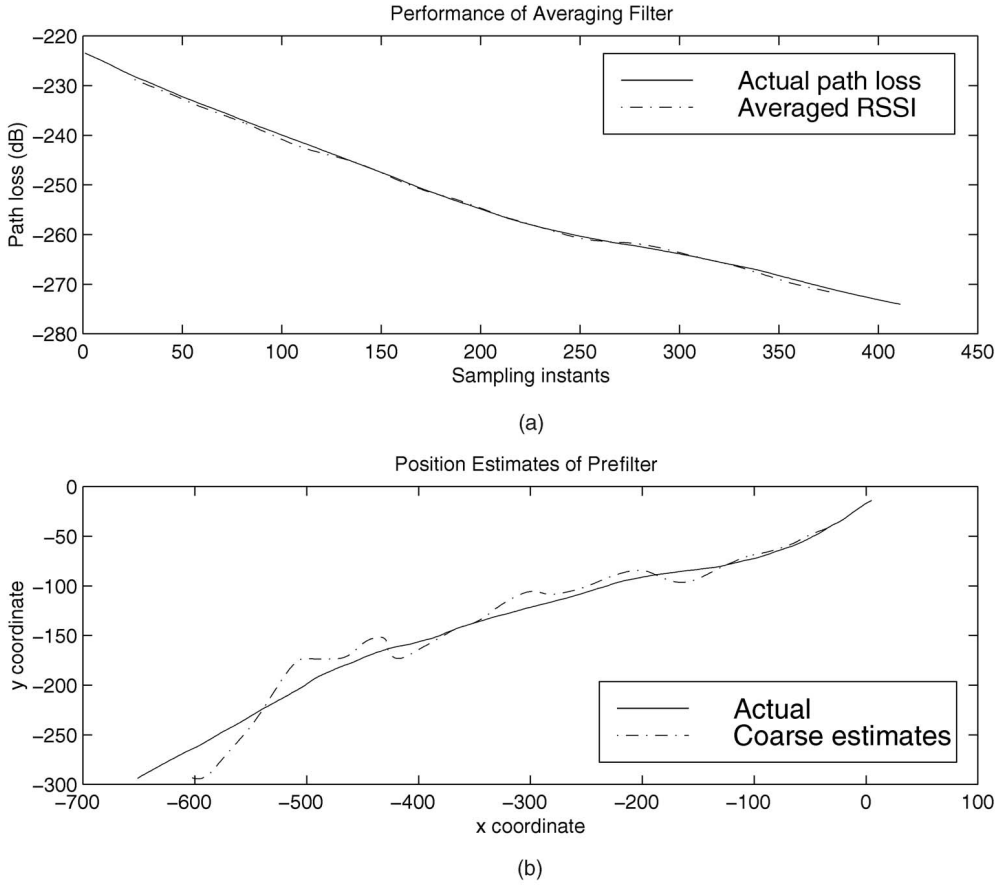

Fig. 2. Performance of prefilter in MT-1 algorithm.

3.1.2 Modified Kalman Filter

The conventional Kalman filter is modified to take into account the discrete command process $\boldsymbol{u}_n$. A Bayesian-based estimator for $\boldsymbol{u}_n$ is integrated into the extended Kalman filter, resulting in the "modified Kalman filter" structure (cf. [1], [20], [21]). In the MT-1 estimator, it is important to note that the input to the modified Kalman filter is the vector of prefiltered observations $\hat{\boldsymbol{o}}_n$, rather than the vector of raw observations $\boldsymbol{o}_n$, as in the LBC algorithm [1].

In the MT-1 algorithm, the Bayesian-based estimator for $\boldsymbol{u}_n$ is an approximation of the conditional mean of $\boldsymbol{u}_n$ given the sequence, $\hat{\boldsymbol{O}}_n = [\hat{\boldsymbol{o}}_1, \cdots, \hat{\boldsymbol{o}}_n]'$, of all prefiltered observations up to time n:

$$\hat{\boldsymbol{u}}_n = \sum_{\boldsymbol{l} \in \mathcal{M}} \boldsymbol{l} \hat{P}\{\boldsymbol{u}_n = \boldsymbol{l} | \hat{\boldsymbol{O}}_n\}, \tag{22}$$

where the conditional probability $P\{\boldsymbol{u}_n = \boldsymbol{l} | \hat{\boldsymbol{O}}_n\}$ is approximated by

$$\hat{P}\{\boldsymbol{u}_n = \boldsymbol{l} | \hat{\boldsymbol{O}}_n\} = cf(\hat{\boldsymbol{o}}_n | \boldsymbol{u}_n = \boldsymbol{l}, \hat{\boldsymbol{O}}_{n-1}) \hat{P}\{\boldsymbol{u}_n = \boldsymbol{l} | \hat{\boldsymbol{O}}_{n-1}\}, \tag{23}$$

with the constant c chosen such that

$$\sum_{\boldsymbol{j} \in \mathcal{M}} \hat{P}\{\boldsymbol{u}_n = \boldsymbol{j} | \hat{\boldsymbol{O}}_n\} = 1.$$

The density $f(\hat{\boldsymbol{o}}_n | \boldsymbol{u}_n = \boldsymbol{l}, \hat{\boldsymbol{O}}_{n-1})$ is approximately Gaussian:

$$\mathcal{N}(H_{pre}(A\hat{\boldsymbol{s}}_{n-1} + B\boldsymbol{l}), H_{pre} M_{n|n-1} H'_{pre}), \tag{24}$$

where

$$H_{pre} = \begin{bmatrix} 1 & 0 & 0 & 0 & 0 & 0 \\ 0 & 0 & 0 & 1 & 0 & 0 \end{bmatrix}. \tag{25}$$

The approximate probability $\hat{P}\{\boldsymbol{u}_n = \boldsymbol{l} | \hat{\boldsymbol{O}}_{n-1}\}$ can be calculated using the transition probability, $a_{\boldsymbol{l},\boldsymbol{j}}$, of the semi-Markov process $\boldsymbol{u}_n$ as follows:

$$\hat{P}\{\boldsymbol{u}_n = \boldsymbol{l} | \hat{\boldsymbol{O}}_{n-1}\} \approx \sum_{\boldsymbol{j} \in \mathcal{M}} a_{\boldsymbol{l},\boldsymbol{j}} P\{\boldsymbol{u}_{n-1} = \boldsymbol{j} | \hat{\boldsymbol{O}}_{n-1}\}. \tag{26}$$

The probability estimates are initialized with the initial discrete command state probabilities $\pi_{\boldsymbol{l}} = P\{\boldsymbol{u}_0 = \boldsymbol{l}\}$ as follows: $\hat{P}\{\boldsymbol{u}_0 = \boldsymbol{l} | \hat{\boldsymbol{O}}_{-1}\} = \pi_{\boldsymbol{l}}$.

The modified Kalman filter is specified as follows: The state estimate at time n is defined by $\hat{\boldsymbol{s}}_{n|n} \triangleq E(\boldsymbol{s}_n | \hat{\boldsymbol{O}}_n)$, with the initialization step $\hat{\boldsymbol{s}}_{0|-1} = \boldsymbol{0}$, where $\boldsymbol{0}$ is the 6×1 vector of all zeros. The Kalman gain matrix is denoted by K_n. The covariance matrix is defined by $M_{n|n-1} \triangleq \mathrm{Cov}(\boldsymbol{s}_n | \hat{\boldsymbol{O}}_{n-1})$ and is initialized by $M_{0|-1} = I_6$.

Recursion steps for MT-1 modified Kalman filter (time n):

1. $\hat{P}\{\boldsymbol{u}_n = \boldsymbol{l} | \hat{\boldsymbol{O}}_{n-1}\} = \sum_{\boldsymbol{j} \in \mathcal{M}} a_{\boldsymbol{l},\boldsymbol{j}} P\{\boldsymbol{u}_{n-1} = \boldsymbol{j} | \hat{\boldsymbol{O}}_{n-1}\}$.
2. $\hat{P}\{\boldsymbol{u}_n = \boldsymbol{l} | \hat{\boldsymbol{O}}_n\} = cf(\hat{\boldsymbol{o}}_n | \boldsymbol{u}_n = \boldsymbol{l}, \hat{\boldsymbol{O}}_{n-1}) \hat{P}\{\boldsymbol{u}_n = \boldsymbol{l} | \hat{\boldsymbol{O}}_{n-1}\}$.
3. $\hat{\boldsymbol{u}}_n = \sum_{\boldsymbol{l} \in \mathcal{M}} \boldsymbol{l} \hat{P}\{\boldsymbol{u}_n = \boldsymbol{l} | \hat{\boldsymbol{O}}_n\}$.
4. $K_n = M_{n|n-1} H'_{pre} (H_{pre} M_{n|n-1} H'_{pre})^{-1}$.
5. $\hat{\boldsymbol{s}}_{n|n} = \hat{\boldsymbol{s}}_{n|n-1} + K_n(\hat{\boldsymbol{o}}_n - H_{pre} \hat{\boldsymbol{s}}_{n|n-1})$[Correction step].
6. $\hat{\boldsymbol{s}}_{n+1|n} = A\hat{\boldsymbol{s}}_{n|n} + B\hat{\boldsymbol{u}}_n$ [Prediction step].

7. $M_{n|n} = (I - K_n H_{pre}) M_{n|n-1} (I - K_n H_{pre})'$.
8. $M_{n+1|n} = A M_{n|n} A' + Q$.

In the recursion part of the filter, the first three steps correspond to the Bayesian-based estimator and the remaining steps implement a conventional Kalman filter.

3.1.3 Extended Kalman Filter

The modified Kalman filter described above provides the mobility state estimates $\hat{\boldsymbol{s}}_{n|n}$ and discrete command estimates $\hat{\boldsymbol{u}}_n$. However, the accuracy of the mobility state estimates $\hat{\boldsymbol{s}}_{n|n}$ is largely dependent on the performance of the prefilter. Since the coarse position estimates are used as the observations for the modified Kalman filter, the best the filter can do is to track the coarse position coordinates. Any inaccuracy and error in the prefilter can cause the estimator to diverge.

To avoid this problem, we have introduced a second (extended) Kalman filter to produce the mobility state estimates. The extended Kalman filter, as shown in Fig. 1a, takes the averaged pilot signal strengths $\hat{\boldsymbol{O}}_n$ as observations and the estimated discrete command states $\hat{\boldsymbol{u}}_n$ from the modified Kalman filter and generates the mobility state estimate $\hat{\boldsymbol{s}}_{n|n}$. The extended Kalman filter consists of a recursion similar to that of Section 3.1.2 (cf. [7]).

Recursion steps for MT-1 extended Kalman filter (time n):

1. $H_n = \frac{\partial h}{\partial \boldsymbol{s}}\Big|_{\boldsymbol{s}=\hat{\boldsymbol{s}}_{n|n-1}}$.
2. $K_n = M_{n|n-1} H_n' (H_n M_{n|n-1} H_n' + R_{res})^{-1}$.
3. $\hat{\boldsymbol{s}}_{n|n} = \hat{\boldsymbol{s}}_{n|n-1} + K_n(\bar{\boldsymbol{o}}_n - h(\hat{\boldsymbol{s}}_{n|n-1}))$[Correction step].
4. $\hat{\boldsymbol{s}}_{n+1|n} = A\hat{\boldsymbol{s}}_{n|n} + B\hat{\boldsymbol{u}}_n$ [Prediction step].
5. $M_{n|n} = (I - K_n H_n) M_{n|n-1} (I - K_n H_n)' - K_n R_{res} K_n'$.
6. $M_{n+1|n} = A M_{n|n} A' + Q$.

The matrix R_{res} is used in the Kalman filter recursion as the covariance matrix of the residual noise in the averaged RSSI's. A suitable matrix for R_{res} is ϵI_3, where $\epsilon \approx 0.01$. The overall performance of the MT-1 mobility estimator in Fig. 1a does not depend strongly on the performance of the prefilter since the residual noise of the prefilter is removed by the extended Kalman filter.

3.2 MT-2 Algorithm

As discussed before, the prefilter used in the MT-1 mobility estimation scheme requires a relatively high frequency of pilot signal samples to be received from the same base station, i.e., one sample per time slot, in order for the averaging filter to reduce the shadowing noise sufficiently. In real-time wireless systems, it is not always possible to meet this requirement on the observation data. At times, it is difficult to obtain a collection of measurements from the same base station because the mobile may move out of range from the base station or an obstruction might make the corresponding signal difficult to measure accurately.

We have developed the MT-2 algorithm as an alternative estimation scheme to deal with scenarios where the prefilter cannot be used to obtain coarse position estimates effectively (cf. Section 3.1.1). Under such scenarios, the discrete command process cannot be estimated accurately by the MT-1 algorithm. As shown in Fig. 3, the MT-2 algorithm consists of a single extended Kalman filter and the discrete command process is treated as additional noise. Here, the total noise covariance matrix is given by

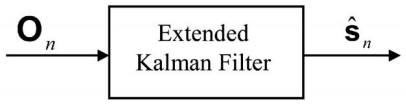

Fig. 3. Block diagram for MT-2 estimator.

$$\tilde{Q} = Q + BE[(\boldsymbol{u}_n - E[\boldsymbol{u}_n])(\boldsymbol{u}_n - E[\boldsymbol{u}_n])']B', \tag{27}$$

where the matrix Q, the covariance matrix of $\boldsymbol{w}_n$, is given in Appendix B. The discrete command process $\boldsymbol{u}_n$ consists of two zero-mean independent semi-Markov processes, so the covariance matrix of $\boldsymbol{u}_n$ is given by

$$E[(\boldsymbol{u}_n - E[\boldsymbol{u}_n])(\boldsymbol{u}_n - E[\boldsymbol{u}_n])'] = \sigma_u^2 I_2, \tag{28}$$

where σ_u^2 is the variance of u_x and u_y. Although the noise process in this case, i.e., $B\boldsymbol{u}_n + \boldsymbol{w}_n$, is not white noise, we ignore the correlation between the noise samples.

The recursion steps in the extended Kalman filter of Fig. 3 are similar to that of the extended Kalman filter described in Section 3.1.3 and are given as follows:

Recursion steps for MT-2 extended Kalman filter (time n):

1. $H_n = \frac{\partial h}{\partial \boldsymbol{s}}\Big|_{\boldsymbol{s}=\hat{\boldsymbol{s}}_{n|n-1}}$.
2. $K_n = M_{n|n-1} H_n' (H_n M_{n|n-1} H_n' + R)^{-1}$.
3. $\hat{\boldsymbol{s}}_{n|n} = \hat{\boldsymbol{s}}_{n|n-1} + K_n(\boldsymbol{o}_n - h(\hat{\boldsymbol{s}}_{n|n-1}))$[Correction step].
4. $\hat{\boldsymbol{s}}_{n+1|n} = A\hat{\boldsymbol{s}}_{n|n}$ [Prediction step].
5. $M_{n|n} = (I - K_n H_n) M_{n|n-1} (I - K_n H_n)' - K_n R K_n'$.
6. $M_{n+1|n} = A M_{n|n} A' + Q$.

3.3 Comparison with LBC Algorithm

The LBC estimator proposed in [1] consists only of the modified Kalman filter, which takes the raw observation data as input and produces mobility state estimates. In this case, the Bayesian-based estimator in the modified Kalman filter approximates the conditional probability density of the pilot signal strengths given the vector of previous observations $\boldsymbol{O}_{n-1}$ with a Gaussian density, i.e., $\mathcal{N}(H_n(A\hat{\boldsymbol{s}}_{n-1} + B\hat{\boldsymbol{u}}_{n-1}), H_n M_{n|n-1} H_n' + R)$ (cf. (43) of [1]). The matrix $M_{n|n-1} \triangleq \mathrm{Cov}(\mathbf{s}_n|\mathbf{O}_{n-1})$ is the covariance matrix and the transformation matrix H_n is given in (20). This assumption turns out to be inaccurate and can lead to divergence of the LBC estimator. An approximation for the conditional probability density function of each element of the observation vector, i.e., the pilot signal strengths $p_{n,i}$, conditioned on the past observations is given in Appendix D.

In our numerical studies (see Section 5), we have found that the Bayesian-based estimator can give inaccurate estimates of $\boldsymbol{u}_n$, primarily due to the approximation of the density $f(\boldsymbol{o}_n|\boldsymbol{O}_{n-1})$ by a Gaussian density. The inaccuracy in the estimates $\hat{\boldsymbol{u}}_n$ leads to divergence of the modified Kalman filter. Consequently, the LBC estimator is not able to track a mobile station that undergoes sudden changes in acceleration. To solve this inherent problem of the LBC estimator, the MT-1 algorithm preprocesses the RSSI measurements using the prefilter to extract the observations suitable for the modified Kalman filter. In MT-1, the modified Kalman filter from the LBC scheme is retained,

but its input consists of coarse position estimates from the prefilter, rather than the raw RSSI measurements. Furthermore, in the MT-1 algorithm, the modified Kalman filter is used only to generate estimates of the discrete command process and a second (extended) Kalman filter is used to yield mobility state estimates using the discrete command estimates and averaged RSSI measurements as inputs. The combination of two Kalman filters in the MT-1 estimator performs much better than the LBC estimator.

In the MT-2 algorithm, the discrete command process $\boldsymbol{u}_n$ is not estimated explicitly, but is treated as additional noise. The structure of the MT-2 estimator is simpler than that of the LBC estimator because it does not include the Bayesian-based estimator for the discrete command process. Thus, the MT-2 algorithm avoids the inherent inaccuracy of the Bayesian-based estimator used in the LBC algorithm. Our numerical results (cf. Section 5) show that MT-2 consistently outperforms the LBC algorithm.

3.4 Mobility Prediction

Under the dynamic mobility model discussed in Section 2, knowledge of the mobility state information at a given time t_0 allows us to predict the mobility state at a time t in the future. The predicted state $\tilde{\boldsymbol{s}}_t$ of a mobile node at time t is given as follows, assuming that the state estimate $\hat{\boldsymbol{s}}_{t_0}$ at time t_0 is available:

$$\tilde{\boldsymbol{s}}_t = A(t-t_0)\hat{\boldsymbol{s}}_{t_0}, \tag{29}$$

where $A(t-t_0) = I_2 \otimes A_1(t-t_0)$. The matrix A_1 is given in (32). The error covariance matrix M_{t-t_0} for the predicted mobility state is given by

$$M_{t-t_0} = A(t-t_0)M_{t_0}A(t-t_0)' + \sigma_u^2 B(t-t_0)B(t-t_0)' + Q(t-t_0), \tag{30}$$

where $M_{t_0} = \mathrm{Cov}(\hat{\boldsymbol{s}}_{t_0})$, σ_u^2 is the variance of u_x and u_y, $B(t-t_0) = I_2 \otimes B_1(t-t_0)$, and $Q(t-t_0) = 2\alpha\sigma_1^2 I_2 \otimes Q_1(t-t_0)$. The matrices B_1 and Q_1 are given in (32) and (33).

Mobility prediction can play a key role in advanced resource management schemes that anticipate the future resource needs of a mobile station. Some promising applications include smooth handoff [1] and fast wireless Internet service provisioning [5]. It is important to note that in using the mobility prediction information (29), one must take into account the degree to which the prediction error grows with time, as indicated by (30).

4 Mobility State Observability

As discussed before, three measurements of pilot signals are needed to locate the mobile unit in two-dimensional space. In real systems, it is not always possible for the mobile to obtain signal measurements from three independent base stations. At times, the mobile may not be able to obtain accurate measurements from at least three pilots as the signals coming from farther base stations may become very weak. In the estimation scheme of Liu et al. [1], the observation set at each sampling instant is assumed to consist of independent RSSI measurements from three different base stations. However, by considering the observability properties of the mobility model, we shall show that mobility tracking can be performed with fewer than three independent RSSI measurements. It is well-known that the Kalman filter can yield meaningful estimates of the system state only if the underlying system is observable [30].

Since the RSSI measurements are nonlinear functions of the mobility state as given in (17), the Jacobian of the transformation function $h(\boldsymbol{s}_n)$, i.e., H_n (cf. (20) and Appendix C) is used to determine observability of the system. The system of (12) is observable over the interval $[n_0, n_1]$ if and only if the columns of the matrix $O_{obs}(n) = H_n\Phi(n_0, n)$ are linearly independent functions of n over $[n_0, n_1]$, where $\Phi(n_0, n)$ is the state-transition matrix of the system (cf. [31]). For the discrete-time realization of the system (cf. (12)), the matrix $\Phi(n_0, n) = A^{n-n_0}$, where A is given in Appendix A. By examining the structure of the observability matrix $O_{obs}(n) = H_n A^{n-n_0}$, as given in Appendix E, the system observability can be characterized more simply as follows:

Proposition 1. *The system of (12) is observable over the interval $[n_0, n_1]$ if and only if $\boldsymbol{x}(n) \neq c\boldsymbol{y}(n)$ for each n over $[n_0, n_1]$, where c is a constant, $\boldsymbol{x}(n) = (x_n - a_1, x_n - a_2, x_n - a_3)$, and $\boldsymbol{y}(n) = (y_n - b_1, y_n - b_2, y_n - b_3)$.*

Proposition 1 implies that the system is observable under fairly general conditions when three independent RSSI measurements are available at each time slot, as should be expected from geometric considerations. When only two RSSI measurements per time slot are available, say from base stations 1 and 2, the observability condition reduces to the inequality of the vectors $(x_n - a_1, x_n - a_2)$ and $c(y_n - b_1, y_n - b_2)$ as functions of n over the interval $[n_0, n_1]$. Therefore, in principle, two independent RSSI measurements per time slot can be sufficient for mobility tracking. Similarly, with only one RSSI measurement, say from base station 1, the observability condition reduces to the inequality of the functions $(x_n - a_1)$ and $c(y_n - b_1)$ over the interval $[n_0, n_1]$. In this case, if the movement of the mobile remains linear for the length of the interval $[n_0, n_1]$, then the observability condition is not satisfied, i.e., $(x_n - a_1) = c(y_n - b_1)$, and estimates of the mobility states cannot be found.

We remark that collecting observations beyond a certain time window has a negligible effect on the observability of the system. The bound on the effective observation window is due to the characteristics of the linear dynamic system model of user's mobility. In this model, the autocorrelation between the random acceleration of the mobile station at time t and $t+\tau$ decays exponentially as τ increases (cf. Section 2). This decay depends on the time-coefficient of acceleration α, with larger α implying faster decay. From Appendix E, one can see that the effect of larger α is to reduce the effective observation window, as subsequent observations beyond the window become less relevant to mobility state estimation at the initial time n_0.

Of course, besides the observability criterion of Proposition 1, there are other factors involved in determining the effectiveness of the mobility tracking. In general, the estimation error is reduced when more independent observations are available. Our numerical results (see Section 5) show that the simplified mobility tracking algorithm MT-2 performs well even when only two independent RSSI measurements are available.

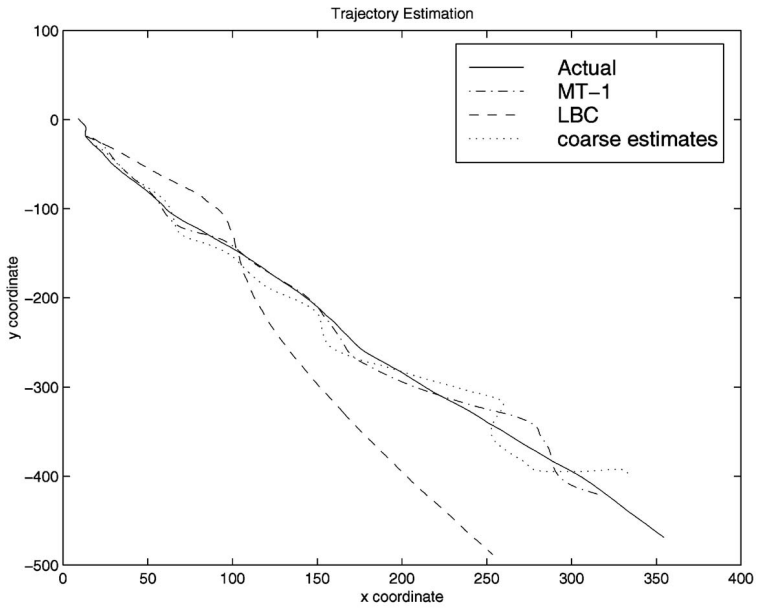

Fig. 4. Performance of MT-1 and LBC algorithms.

5 Numerical Results

In our numerical experiments, random mobile trajectories are generated in Matlab using the dynamic state model given in (12). The position coordinates are specified in units of meters. The parameters determining the autocorrelation function of the random acceleration process $\boldsymbol{r}(t)$ are set as follows (cf. (4)): $\alpha = 1000\ \mathrm{s}^{-1}$ and $\sigma_1 = 1$ dB. The covariance matrix R of $\boldsymbol{\psi}_n$ (cf. (17)) is determined by setting the parameter $\sigma_\psi = 6$ dB. The state vector $\boldsymbol{s}(t)$ is initialized to the zero vector.

The discrete command processes $u_x(t)$ and $u_y(t)$ are independent semi-Markov processes, each taking on five possible levels of acceleration comprising the set $\mathcal{L} = \{-5, -2.5, 0, 2.5, 5\}$ in units of $\mathrm{m/s}^2$. This set of acceleration levels is capable of generating a wide range of dynamic motion. We refer to this selection as the *high mobility scenario*. The sampling interval is set to $T = 0.1$s. The initial probability vector $\boldsymbol{\pi}$ for the HSMM is initialized to the uniform distribution. The total duration of each sample trajectory is $N = 600$ sample points, which corresponds to 2 minutes. The elements of the transition probability matrix A_h are initialized to a common value of $1/5$. We assume that the dwell times in each state are uniformly distributed with a common mean value of 2 s. The parameter κ_i is assumed to be zero for all cells i.

Fig. 4 shows a typical sample mobile trajectory,[8] generated by the dynamic state model with the given parameter values. The figure also shows estimated trajectories obtained from the LBC algorithm and the MT-1 algorithm, respectively. The figure shows that the LBC algorithm fails to track the actual trajectory, particularly when there are sharp or sudden changes in direction. We remark that standard GPS techniques would also fail to track the sudden accelerations produced by the dynamic state model with the given parameter settings. On the other hand, MT-1 is able to follow the curves of the actual trajectory with reasonably good accuracy. We remark that the sample trajectories corresponding to the specified parameter values are considerably more dynamic than those of an actual mobile station in a live network environment. They provide a good benchmark to evaluate the robustness and accuracy of mobility tracking algorithms.

We use root mean squared error (RMSE) as a figure of merit to compare a given trajectory $\{x_n, y_n\}$ and its estimated trajectory $\{\hat{x}_n, \hat{y}_n\}$:

$$\mathrm{RMSE} = \sqrt{\frac{1}{N}\sum_{n=1}^{N}[(\hat{x}_n - x_n)^2 + (\hat{y}_n - y_n)^2]}. \qquad (31)$$

Table 1 shows the sample mean and variance of the RMSE statistic computed using more than 500 independently generated sample trajectories. We denote the selection of acceleration levels between -5 to $5\ \mathrm{m/s}^2$ as the high mobility scenario in Table 1. To evaluate the comparative performance of MT-1 and MT-2 with LBC under low mobility conditions more typical for actual cellular networks, we also perform a set of simulations for the discrete command levels selected from $\mathcal{L} = \{-0.5, -0.25, 0, 0.25, 0.5\}\mathrm{m/s}^2$. The respective results are listed under the "low mobility scenario" column in Table 1. In the scenarios of Table 1, three base stations provide independent RSSI measurements at each time slot. The performance of the mobility tracking algorithms is evaluated when the parameter σ_ψ is set to 6 dB and 8 dB. Recall that σ_ψ determines the covariance matrix of the observation noise (cf. (17)).

Table 1 provides a quantitative comparison of the relative merits of the MT-1, MT-2, and LBC estimators, which confirms the qualitative implications of Fig. 4. The table shows that under perfect observation conditions for prefiltering, the MT-1 estimator achieves the best performance. The MT-2 estimator performs reasonably well and clearly outperforms the LBC estimator. The performance degradation of the LBC estimator is observed to be much greater than that of

8. The starting point is at $(0, 0)$.

TABLE 1
RMSE of Tracking Algorithms

Tracking Algorithm	σ_ψ	Low Mobility Scenario		High Mobility Scenario	
	(dB)	μ_{RMSE} (m)	σ_{RMSE} (m)	μ_{RMSE}(m)	σ_{RMSE} (m)
LBC	6	35.87	9.94	42.04	10.68
MT-1	6	6.42	2.64	6.27	2.75
MT-2	6	17.88	4.84	13.36	5.37
SMC	6	35.15	10.15	28.47	12.06
LBC	8	37.34	10.3	42.86	11.91
MT-1	8	6.5	2.44	6.48	2.66
MT-2	8	18.69	4.84	14.07	5.61
SMC	8	36.6	10.47	29.13	13.12

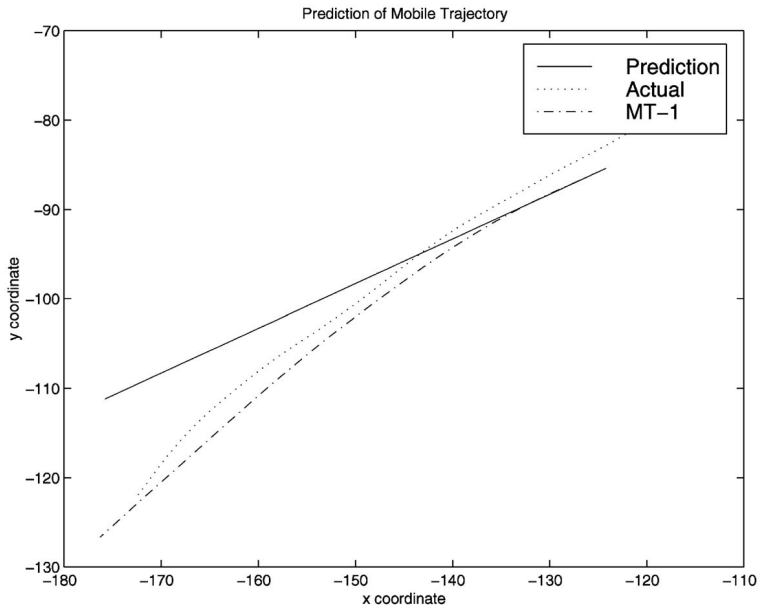

Fig. 5. Example of mobility prediction.

MT-1 and MT-2 when the noise level in the observation data is increased.

Table 1 also shows performance degradation for the LBC estimator when the trajectories are more dynamic although the other tracking algorithms show stable or even better performance for the high mobility scenario. In our numerical analysis, we also performed simulations for the lower mobility conditions and MT-1 and MT-2 consistently perform better than LBC. We conclude that MT-1 and MT-2 achieve better performance than LBC over a wide range of mobility scenarios and wireless propagation environments.

Table 1 also provides a quantitative performance comparison of MT-1 and MT-2 with the sequential Monte Carlo (SMC) approach to mobility tracking (cf. [2]). The number of samples is selected to be 800 corresponding to the best estimator described in [2]. The initial mobility state samples are initialized as zero vectors and their respective weights are initialized to unity. Table 1 shows that although SMC provides better performance than LBC, the MT-1 and MT-2 estimators both outperform the SMC estimator for all tested scenarios of mobility and propagation environments. The MT-1 and MT-2 estimators are also computationally simpler than the SMC algorithm.

Fig. 5 shows a sample trajectory of a mobile user in a cellular network, along with the estimated and predicted trajectories under the MT-1 algorithm. The predicted trajectory is a straight line that starts in the upper right-hand corner of the figure at the point $(-125, -85)$. Observe that the predicted trajectory initially stays close to the estimated trajectory and then deviates from it over time. The deviation indicates the increase in prediction error or, more precisely, the prediction uncertainty. An important point to be noted here is that although prediction error increases with time, the estimation error is independent of time once the Kalman filter reaches the steady state.

The performance of the mobility tracking algorithms under a scenario of limited observation data is shown in Fig. 6. In the scenario for Fig. 6, the mobile unit selects, in each

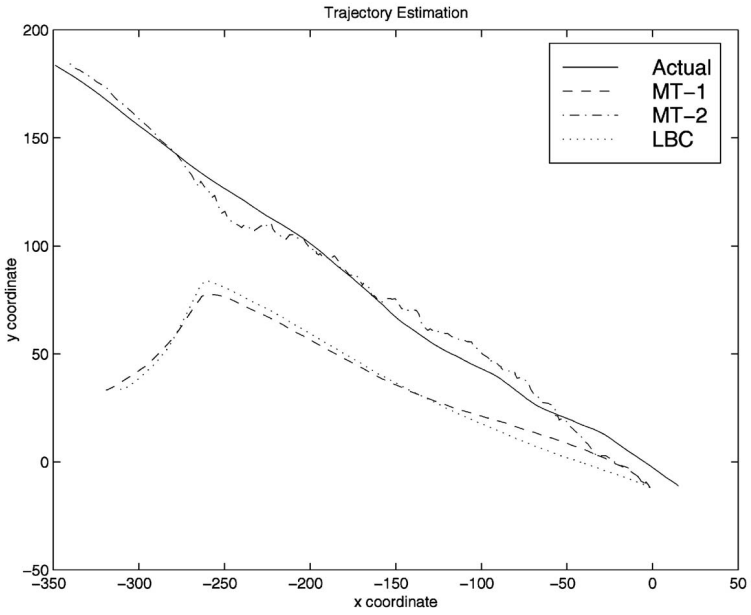

Fig. 6. Performance of mobility tracking algorithms under limited observation data.

time slot, three RSSI measurements from a set of nine base stations in its vicinity to form an *active set*. In practice, the three strongest RSSI measurements would be selected. In order to simulate the effect of the dynamic changes to the active set of three base stations over time, the active set changes from time slot to time slot in the sequence $\{1,2,3\}$, $\{4,5,6\}$, $\{7,8,9\}$, and repeats. Thus, an RSSI measurement from a given base station is available only once every three time slots. This scenario was chosen to reflect similar patterns observed in test drives of an actual CDMA network. As can be seen in Fig. 6, only the MT-2 algorithm is able to track the mobile trajectory accurately. In this case, the prefilter in the MT-1 algorithm is ineffective, resulting in inaccurate discrete command estimates. In the LBC algorithm, the discrete command estimates are also inaccurate, although for a different reason (cf. Section 3.3).

In Fig. 7a, a sample trajectory is estimated using the MT-2 algorithm for the following different cases of observation data availability:

- w 1 obs, 1 BS: One RSSI measurement per time slot from one base station.
- w 1 obs, 2 BS: One RSSI measurement per time slot alternately from two base stations.
- w 2 obs: Two independent RSSI measurements per time slot.
- w 3 obs: Three independent RSSI measurements per time slot.

The initial position of the sample trajectory of Fig. 7a is shown by "*" whereas the estimated trajectories are initialized at the origin. When three independent RSSI measurements are available per time slot, the MT-2 estimator converges fastest to the true trajectory. When two RSSI measurements are available per time slot, convergence occurs more slowly. The worst case shown is when only one observation from a single base station is available throughout the course of trajectory estimation. In this case, the MT-2 estimator fails to track the given trajectory.

An explanation of this last case in terms of the observability arguments of Section 4 is given as follows: Since $\alpha = 1000\ s^{-1}$ and $T = 0.1\ s$, the observation window is approximately 5, i.e., 0.5 seconds (see Appendix E). During this short time window, the movement of the mobile remains approximately linear and, consequently, the system is not observable (cf. Section 4). However, the estimation performance improves significantly if two base stations supply one observation per sampling interval alternately. Thus, involving RSSI measurements from another base station helps to satisfy the observability criterion.

For the cases where fewer than three observations are available, the estimation performance is largely determined by the observability criteria. The estimators are not dependable for the intervals when the system is unobservable. Also, more observations provide more redundancy to overcome the observation noise. In the case where three observations are available, the estimator performs equally well regardless of whether or not prior knowledge of the mobile (i.e., initial location) is known.

In Fig. 7b, the performance of MT-2 is shown for different numbers of observations available at each sampling instant when some prior knowledge of the initial position of the mobile unit is given. This situation may occur when, for example, the number of independent RSSI measurements suddenly reduces from three to two and the most recent position estimate effectively initializes the future iterations of the tracking algorithm on the reduced observation data set. In practice, pilot signals from one or more of the base stations in the active set may become corrupted due to path obstructions during a call and, hence, the active set may have to be reduced in size. With prior knowledge of the mobile's position, the availability of two independent RSSI measurements yields similar performance as in the case with three independent RSSI measurements. When only one observation is available in alternate time slots from two base stations, we observe a reduction in tracking performance. As

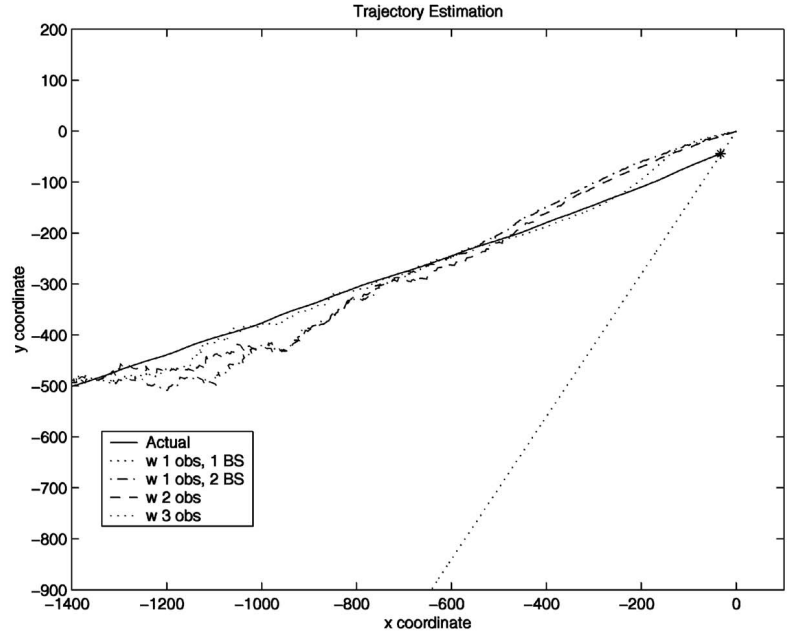

(a)

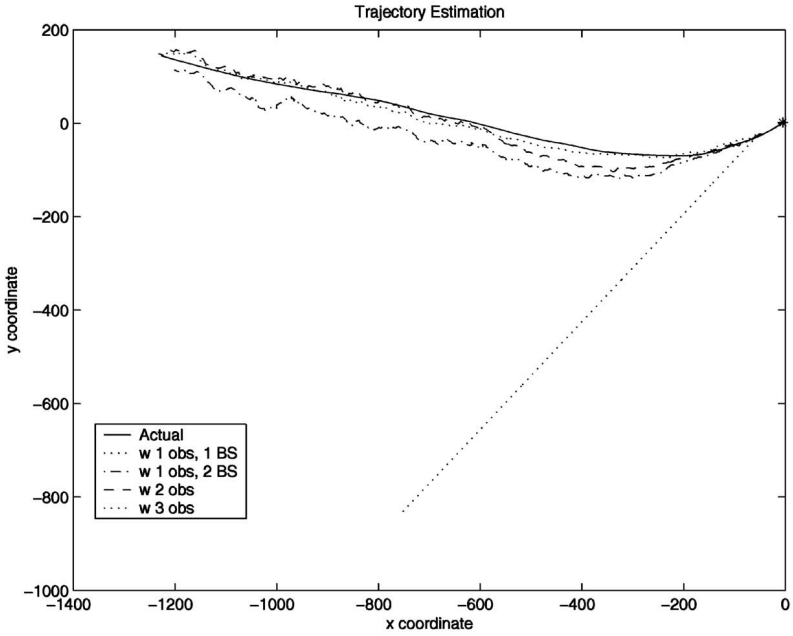

(b)

Fig. 7. Performance of MT-2 algorithm with different observation data. (a) When no prior knowledge of initial location is available. (b) When prior knowledge of initial location is available.

shown in Fig. 7b, when observations are available only from a single base station, the MT-2 estimator diverges, even though the initial position of the mobile is given.

6 Conclusion

We have proposed two algorithms, called MT-1 and MT-2, for mobility tracking in cellular networks using RSSI measurements. Both MT-1 and MT-2 are based on a dynamic system model of mobility and employ variants of the Kalman filter in the estimation process. The mobility model, originally proposed for tracking targets in tactical weapons systems, can capture a large range of mobility by modeling acceleration as driven by a discrete command process. The proposed mobility tracking algorithms are able to follow mobile trajectories more accurately than the LBC algorithm proposed earlier by Liu et al. [1]. A defect of the LBC algorithm is that it relies on the incorrect assumption that the probability density of the current observation at any time conditioned on the previous observations is Gaussian. As a result, the LBC algorithm can diverge even under relatively simpler mobility scenarios.

The MT-1 algorithm avoids this problem by 1) employing a prefilter to obtain coarse position estimates prior to the

application of the modified Kalman filter and 2) decoupling mobility state estimation from estimation of the discrete command process. The MT-2 algorithm consists of a single extended Kalman filter, wherein the discrete command process is treated as additional noise. Under certain scenarios of limited observation data where MT-1 fails, MT-2 is able to track mobility with adequate accuracy. In all of our numerical experiments, both MT-1 and MT-2 outperform the LBC algorithm by a large margin. The MT-1,2 algorithms also compare favorably against the SMC mobility tracking algorithm proposed in [2].

Requirements on the observation data for the tracking algorithms were also investigated and observability arguments from systems theory suggested that mobility tracking could be achieved with fewer than three independent RSSI measurements from base stations. Our numerical results showed that two independent RSSI measurements were sufficient for mobility tracking but a single RSSI measurement was not. The proposed mobility tracking algorithms can be used in mobility-based resource allocation schemes such as fast IP handoff [3] and precaching of Web proxy servers [5].

Appendix A

State Equation Matrices

The matrices A and B are given by:[9]

$$A = e^{\tilde{A}T}, B = \int_t^{t+T} e^{\tilde{A}(t+T-\tau)}\tilde{B}d\tau.$$

Using standard techniques from matrix algebra, the matrices can be written as

$$A = I_2 \otimes A_1(T), \quad B = I_2 \otimes B_1(T),$$

where

$$A_1(T) = \begin{bmatrix} 1 & T & a \\ 0 & 1 & b \\ 0 & 0 & e^{-\alpha T} \end{bmatrix}, \quad B_1(T) = \begin{bmatrix} c \\ \alpha a \\ \alpha b \end{bmatrix}, \tag{32}$$

and

$$\begin{aligned} a &= (-1 + \alpha T + e^{-\alpha T})/\alpha^2, \\ b &= (1 - e^{-\alpha T})/\alpha, \\ c &= (1 - \alpha T + \frac{\alpha^2}{2}T^2 - e^{-\alpha T})/\alpha^2. \end{aligned}$$

Appendix B

Covariance Matrix of Discrete White Noise

The matrix Q is given by[10]

$$Q = 2\alpha\sigma_1^2 I_2 \otimes Q_1(T),$$

where $Q_1(T) = [q_{ij}]$ is a symmetric 3×3 matrix with upper triangular entries given as follows:

$$\begin{aligned} q_{11} &= (1 - e^{-2\alpha T} + 2\alpha T + 2\alpha^3 T^3/3 - 2\alpha^2 T^2 - 4\alpha T e^{-\alpha T}) \\ &\quad /(2\alpha^5), \\ q_{12} &= (e^{-2\alpha T} + 1 - 2e^{-\alpha T} + 2\alpha T e^{-\alpha T} - 2\alpha T + \alpha^2 T^2)/(2\alpha^4), \\ q_{13} &= (1 - e^{-2\alpha T} - 2\alpha T e^{-\alpha T})/(2\alpha^3), \\ q_{22} &= (4e^{-\alpha T} - 3 - e^{-2\alpha T} + 2\alpha T)/(2\alpha^3), \\ q_{23} &= (e^{-2\alpha T} + 1 - 2e^{-\alpha T})/(2\alpha^2), \\ q_{33} &= (1 - e^{-2\alpha T})/(2\alpha). \end{aligned} \tag{33}$$

Appendix C

Transformation Matrix of Linearized Observations

The matrix H_n in the linearized observation (19) is given by

$$H_n = -5\gamma \begin{bmatrix} \boldsymbol{h}_{n,1} \\ \boldsymbol{h}_{n,2} \\ \boldsymbol{h}_{n,3} \end{bmatrix},$$

where $\boldsymbol{h}_{n,i}$ is the ith row of H_n with

$$\boldsymbol{h}_{n,i} = \frac{2}{d_{n,i}^2}(x_n - a_i, 0, 0, y_n - b_i, 0, 0),$$

for $i = 1, 2, 3$.

Appendix D

Probability Density Function of RSSI

The conditional probability density function (pdf) of the mobility state vector conditioned on the past observations is approximately Gaussian (cf. [1]), i.e.,

$$f(\boldsymbol{s}_n|\boldsymbol{O}_{n-1}) \sim \mathcal{N}(A\hat{\boldsymbol{s}}_{n-1} + B\hat{\boldsymbol{u}}_{n-1}, M_{n|n-1}), \tag{34}$$

where $\boldsymbol{O}_{n-1} = (\boldsymbol{o}_{n-1}, ..., \boldsymbol{o}_1)$ and the matrix $M_{n|n-1} \triangleq \mathrm{Cov}(\boldsymbol{s}_n|\boldsymbol{O}_{n-1})$ is the covariance matrix. Thus, the position coordinates of the mobile $(x_n,\ y_n)$ conditioned on $\boldsymbol{O}_{n-1}$ can be approximated by Gaussian random variables with (mean, variance) given by (μ_x, σ_x^2) and (μ_y, σ_y^2), respectively. These quantities can be obtained from the mean and covariance matrices of the mobility state vector as defined in (34). The pdf of the distance, $d_{n,i}$, of the mobile from a base station in cell i at sampling time n is given by

$$f_{d_{n,i}}(\lambda) = \frac{\lambda}{2\pi\sigma_x\sigma_y} g(\lambda),$$

where

$$g(\lambda) \triangleq \int_0^{2\pi} \exp \left(\frac{-(\lambda\cos\theta - (\mu_x - a_i))^2}{2\sigma_x^2} - \frac{(\lambda\sin\theta - (\mu_y - b_i))^2}{2\sigma_y^2} \right) d\theta,$$

and (a_i, b_i) are the coordinates of base station i. The path loss for cell i is $h_i = \kappa_i - 10\gamma\log(d_{n,i})$, where the pdf of h_i is given by

9. The expression for the matrix B given in (36) of [1] is incorrect.
10. This expression is equivalent to (37) in [1].

$$f_{h_i}(\eta) = \frac{1}{20\gamma\pi\sigma_x\sigma_y} e^{\frac{\kappa_i-\eta}{5\gamma}} g\Big(e^{\frac{\kappa_i-\eta}{10\gamma}}\Big).$$

The conditional pdf of the pilot signal strength $p_{n,i}$ given the previous observations is approximated by

$$f_{p_{n,i}}(\nu|\boldsymbol{O}_{n-1}) = \frac{1}{20\gamma\pi\sigma_x\sigma_y} \frac{1}{\sqrt{2\pi\sigma_\psi^2}} \int_{-\infty}^{\infty} e^{\frac{\kappa_i-\eta}{5\gamma}} e^{\frac{-(\nu-\eta)^2}{2\sigma_\psi^2}} g\Big(e^{\frac{\kappa_i-\eta}{10\gamma}}\Big) d\eta.$$

The above expression cannot be evaluated in closed form. Numerical integration might be a possible solution, but is time-consuming and, therefore, unsuitable for real-time mobility estimation.

APPENDIX E
OBSERVABILITY MATRIX

The observability matrix $O_{obs}(n) = H_n A^{n-n_0}$ can be written as

$$O_{obs}(n) = -10\gamma[O_{obs,x}(n), O_{obs,y}(n)], \tag{35}$$

where

$$O_{obs,x}(n) = \begin{bmatrix} p_{x,1} & p_{x,1}(n-n_0)T & p_{x,1}p_n \\ p_{x,2} & p_{x,2}(n-n_0)T & p_{x,2}p_n \\ p_{x,3} & p_{x,3}(n-n_0)T & p_{x,3}p_n \end{bmatrix} \tag{36}$$

and $O_{obs,y}(n)$ is defined similarly, except that the subscript x is replaced by y. Here,

$$p_{x,i} = \frac{x_n - a_i}{d_{n,i}^2},\ p_{y,i} = \frac{y_n - b_i}{d_{n,i}^2}, \quad i = 1,2,3,$$

and

$$p_n = \frac{1}{\alpha^2}\Big(-1 + (n-n_0)\alpha T + e^{-(n-n_0)\alpha T}\Big).$$

We remove the constant -10γ in (35) and perform the following column operations on $O_{obs}(n)$, where C_i denotes the ith column:

1. $C_3 = \alpha^2 C_3$ and $C_6 = \alpha^2 C_6$, and
2. $C_3 = C_3 + C_1 - \alpha C_2$ and $C_6 = C_6 + C_4 - \alpha C_5$

to obtain a reduced matrix $\tilde{O}_{obs}(n) = [\tilde{O}_{obs,x}(n), \tilde{O}_{obs,y}(n)]$, where

$$\tilde{O}_{obs,x}(n) = \begin{bmatrix} p_{x,1} & p_{x,1}(n-n_0)T & p_{x,1}e^{-(n-n_0)\alpha T} \\ p_{x,2} & p_{x,2}(n-n_0)T & p_{x,2}e^{-(n-n_0)\alpha T} \\ p_{x,3} & p_{x,3}(n-n_0)T & p_{x,3}e^{-(n-n_0)\alpha T} \end{bmatrix} \tag{37}$$

and $\tilde{O}_{obs,y}(n)$ is defined similarly.

Note that the third and sixth columns of $\tilde{O}_{obs}(n)$ consist of exponentials which go to zero as $(n-n_0)$ increases. This implies a limit on the effective observation window size. For example, if $\alpha = 1000\ s^{-1}$ and $T = 0.1\ s$, then $e^{-(n-n_0)\alpha T} \approx 0$ for $(n-n_0) = 5$, which implies that only the first five observations from n_0 are useful for estimating the system state at time n_0.

From (37), one sees that observability of the system, or the linear independence of columns of $\tilde{O}_{obs}(n)$ over an observation interval $[n_0, n_1]$, depends on the position coordinates $(x_n,\ y_n)$ of the mobile. The system is observable over the interval $[n_0, n_1]$ if and only if $\boldsymbol{x}(n) \neq c\boldsymbol{y}(n)$ for each n over $[n_0, n_1]$, where c is a constant and $\boldsymbol{x}(n)$ and $\boldsymbol{y}(n)$ are the vector functions $\boldsymbol{x}(n) = (x_n - a_1, x_n - a_2, x_n - a_3)$ and $\boldsymbol{y}(n) = (y_n - b_1, y_n - b_2, y_n - b_3)$.

ACKNOWLEDGMENTS

This work was supported by the US National Science Foundation under Grant No. ACI-0133390 and by a grant from the TRW Foundation.

REFERENCES

[1] T. Liu, P. Bahl, and I. Chlamtac, "Mobility Modeling, Location Tracking, and Trajectory Prediction in Wireless ATM Networks," *IEEE J. Selected Areas in Comm.,* vol. 16, pp. 922-936, Aug. 1998.

[2] Z. Yang and X. Wang, "Joint Mobility Tracking and Hard Handoff in Cellular Networks via Sequential Monte Carlo Filtering," *Proc. IEEE INFOCOM '02,* vol. 2, pp. 968-975, June 2002.

[3] J. Kempf, J. Wood, and G. Fu, "Fast Mobile IPv6 Handover Packet Loss Performance," *Proc. IEEE Wireless Networking and Comm. Conf. (WCNC '03),* Mar. 2003.

[4] Y. Gwon, G. Fu, and R. Jain, "Fast Handoffs in Wireless LAN Networks Using Mobile Initiated Tunneling Handoff Protocol for IPv4 (MITHv4)," *Proc. IEEE Wireless Networking and Comm. Conf. (WCNC 2003),* pp. 1248-1252, Mar. 2003.

[5] H. Kobayashi, S.Z. Yu, and B.L. Mark, "An Integrated Mobility and Traffic Model for Resource Allocation in Wireless Networks," *Proc. Third ACM Int'l Workshop Wireless Mobile Multimedia,* pp. 39-47, Aug. 2000.

[6] J.B. Tsui, *Fundamentals of Global Positioning System Receivers: A Software Approach.* New York: John Wiley & Sons, 2000.

[7] R.G. Brown and P.Y. Hwang, *Introduction to Random Signals and Applied Kalman Filtering.* third ed., New York: John Wiley & Sons, 1997.

[8] G.M. Djuknic and R.E. Richton, "Geo-Location and Assisted GPS," *Computer,* vol. 34. pp. 123-125, Feb. 2001.

[9] F.V. Diggelen, "Indoor GPS Theory and Implementation," *Proc. IEEE Position Location and Navigation Symp. 2002,* pp. 240-247, 2002.

[10] K.C. Ho and Y.T. Chan, "Solution and Performance Analysis of Geolocation by TDOA," *IEEE Trans. Aerospace and Electronic Systems,* pp. 1311-1322, Oct. 1993.

[11] P. Deng and P.Z. Fan, "An AOA Assisted TOA Positioning System," *Proc. World Computer Congress-Int'l Conf. Communication Technology (WCC-ICCT '00),* vol. 2, pp. 1501-1504, 2000.

[12] L. Cong and W. Zhuang, "Hybrid TDOA/AOA Mobile User Location for Wideband CDMA Cellular Systems," *IEEE Trans. Wireless Comm.,* vol. 1, pp. 1439-1447, July 2002.

[13] P. Bahl and V.N. Padmanabhan, "RADAR: An In-Building RF-Based User Location and Tracking System," *Proc. IEEE INFOCOM '00,* vol. 2, pp. 775-784, Mar. 2000.

[14] P.C. Chen, "A Cellular Based Mobile Location Tracking System," *Proc. IEEE Vehicular Technology Conf. (VTC '99),* pp. 1979-1983, 1999.

[15] D. Gu and S.S. Rappaport, "A Dynamic Location Tracking Strategy for Mobile Communication Systems," *Proc. Vehicular Technology Conf. (VTC '98),* pp. 259-263, 1998.

[16] Y. Lin and P. Lin, "Performance Modeling of Location Tracking Systems," *Mobile Computing and Comm. Rev.,* vol. 2, no. 3, pp. 24-27, 1998.

[17] M. Hellebrandt and R. Mathar, "Location Tracking of Mobiles in Cellular Radio Networks," *IEEE Trans. Vehicular Technology,* vol. 48, pp. 1558-1562, Sept. 1999.

[18] I.F. Akyildiz, Y.B. Lin, W.R. Lai, and R.J. Chen, "A New Random Walk Model for PCS Networks," *IEEE J. Selected Areas in Comm.,* vol. 18, no. 7, pp. 1254-1260, 2000.

[19] K.K. Leung, W.A. Massey, and W. Whitt, "Traffic Models for Wireless Communication Networks," *IEEE J. Select. Areas in Comm.,* vol. 12, pp. 1353-1364, Oct. 1994.

[20] R.A. Singer, "Estimating Optimal Tracking Filter Performance for Manned Maneuvering Targets," *IEEE Trans. Aerospace and Electronic Systems,* vol. 6, pp. 473-483, July 1970.

[21] R.L. Moose, H.F. Vanlandingham, and D.H. McCabe, "Modeling and Estimation for Tracking Maneuvering Targets," *IEEE Trans. Aerospace and Electronic Systems,* vol. 15, pp. 448-456, May 1979.

[22] B.L. Mark and Z.R. Zaidi, "Robust Mobility Tracking for Cellular Networks," *Proc. IEEE Int'l Conf. Comm. (ICC '02),* vol. 1, pp. 445-449, May 2002.
[23] J.J. Caffery Jr., *Wireless Location in CDMA Cellular Radio Systems.* Norwell, Mass.: Kluwer Academic, 1999.
[24] R.E. Bellman, *Introduction to Matrix Analysis.* New York: McGraw-Hill, 2nd ed. 1970.
[25] G.L. Stuber, *Principles of Mobile Communication.* second ed., Mass.: Kluwer Academic, 2001.
[26] M. Gudmundson, "Correlation Model for Shadowing Fading in Mobile Radio Systems," *Electronic Letters,* vol. 27, pp. 2145-2146, Nov. 1991.
[27] H. Suzuki, "A Statistical Model for Radio Propagation," *IEEE Trans. Comm.,* vol. 25, pp. 673-680, July 1977.
[28] J.W. Mark and W. Zhuang, *Wireless Communications and Networking.* Prentice Hall, 2003.
[29] *DeciBel Planner, Planet General Model Technical Notes.* Northwood Technologies Inc., Sept. 2001.
[30] B. Southall, B.F. Buxton, and J.A. Marchant, "Controllability and Observability: Tools for Kalman Filter Design," *Proc. British Machine Vision Conference (BMVC '98),* vol. 1, pp. 164-173, 1998.
[31] T. Kailath, *Linear Systems* Englewood Cliffs, N.J.: Prentice-Hall, Inc., 1980.

Zainab R. Zaidi (S'00) received the BE degree in electrical engineering from NED University of Engineering and Technology, Karachi, Pakistan in 1997. She received the MS degree in electrical engineering and the PhD in electrical and computer engineering from George Mason University, Fairfax, Virginia in 1999 and 2004, respectively. Currently, she is working on her postdoctoral studies in the Department of Electrical and Computer Engineering at George Mason University. Her research involves geolocation, mobility tracking techniques, and their applications to security and quality-of-service aspects of cellular and mobile ad hoc networks. She is a student member of the IEEE.

Brian L. Mark (M'91) received the BASc degree in computer engineering with an option in mathematics from the University of Waterloo, Canada, in 1991 and the PhD degree in electrical engineering from Princeton University, Princeton, in 1995. He was a research staff member at the C&C Research Laboratories, NEC US, from 1995 to 1999. In 1999, he was on part-time leave from NEC as a visiting researcher at Ecole Nationale Supérieure des Télécommunications in Paris, France. In 2000, he joined the Department of Electrical and Computer Engineering at George Mason University, where he is currently an assistant professor. His main recent research interests lie broadly in the design, modeling, and analysis of communication systems, communication networks, and computer systems. He was corecipient of the best conference paper award for IEEE Infocom '97. He received a US National Science Foundation CAREER Award in 2002. He is a member of the IEEE.